Progress In Electromagnetics Research, PIER 86, 259–275, 2008

DESIGN AND CONSTRUCTION OF WIDEBAND VNA GROUND-BASED RADAR SYSTEM WITH REAL AND SYNTHETIC APERTURE MEASUREMENT CAPABILITIES

K.-S. Lim and V.-C. Koo

Multimedia University
Cyberjaya 63100, Malaysia

Abstract—This paper presents the design and construction of an advanced wideband, automated radar system. With the aid of Vector Network Analyzer (VNA), a wideband ground-based system can be achieved with proper Radio Frequency (RF) circuitry integration. The RF circuitry is designed specifically to configure the proposed system to be able to measure full linear polarimetric scattering matrices of the area of interest. Besides, quasi-monostatic horn antenna configuration is chosen to transmit and receive the electromagnetic wave. The goal of this paper is to demonstrate the real and synthetic aperture capabilities of the system in outdoor measurement with the microwave frequency range from 2 to 7 GHz. Coupled with the integration of the Automatic Antenna Positioning System (AAPS), the constructed system is able to perform real and synthetic aperture radar measurements. A series of measurement was done on real aperture radar measurement using point target for validity purpose. The overall results show good agreement with the theoretical values. On the other hand, the proposed system is capable to performing a radar imaging measurement. A preliminary analysis is done on a 45 days old rice field. A three dimensional (3-D) radar image has also been constructed successfully with Range Migration Technique (RMA). The result shows good potential of the system in constructing radar imaging of natural target.

1. INTRODUCTION

Over the past few decades, several space-borne synthetic aperture radars have been operating and used excessively such as ERS-1, ERS-2, JERS-1 and RADARSAT. They are now providing commercial radar images from the space, which allow extraction of unique information of

the earth terrain. However, measured result from ground-based radar system is still of great demand to the remote sensing community. One of the main reasons is that the ground measured terrain microwave signature is available all the time without having to rely on the rotation of the satellite. Hence, several ground-based microwave remote sensing systems have been constructed to provide accurate and reliable ground truth information to better understand the earth terrain.

In the past, extensive research on the distribution of sources of the backscattering within vegetation canopies [1–16] has been carried out and the experiments on agricultural fields have been performed using ground-based radar systems [17–19]. Field scatterometers had been utilized at 10 GHz (X-band) [20, 21] while other studies [7, 22–25] had used the 4.75-GHz field scatterometers and the microwave scatterometer C-band (MS-C). Le Toan [26, 27] investigated the radar backscatter from the rice crops by using an airborne X-Band Synthetic Aperture Radar (SAR), VARAN-S, operating in HH and VV at the incident angle of 0° to 60°. On the other hand, Kurosu [28] had also conducted an experiment on the entire rice growth cycle with VV polarization at the incident angle of 23° while Kim Soo Bum [29] performed the measurements using X-band scatterometer. These studies agree that the observed backscatter is a combination of the ground backscatter attenuated by the canopy layer and the backscatter from the canopy.

A ground-based microwave remote sensing system was designed using inexpensive FMCW and it was operated in narrow bandwidth [30, 31]. In the recent decade, the development of ground-based microwave remote sensing system focuses on wideband system construction. This is most likely due to the availability of Vector Network Analyzer (VNA) at affordable price. Therefore, the wideband radar system is proposed to offer a better design and configuration in terms of operating, setup time, measurement time and mobility. The system is constructed using VNA as the main measurement instrument.

In this paper, we present not only the measurement of point target for calibration purpose and a measurement from rice field, but also the image reconstruction of the rice field using the proposed radar system. Over the past few decades, there were a considerable number of researchers who investigated on the 2-D and 3-D image reconstruction techniques [32–44]. The image reconstruction technique, Range Migration Algorithm is implemented with the aim to produce 3-D radar image. This technique is chosen because of its suitability in space borne SAR platform in stripmap mode. The basic idea from 2-D processing had lead to the extension of 3-D image reconstruction.

The paper is organized as follows. Section 2 describes the design

and configuration of the VNA ground-based radar system with its detailed specification. The ground truth measurement procedure for real and synthetic aperture measurements are explained in Section 3. This is followed by the discussion of the results of the static point target and scanning measurements in Section 4. In Section 5, we conclude and summarize this paper.

2. DESIGN AND CONSTRUCTION OF PROPOSED RADAR SYSTEM

The main objective of this system construction is to design and develop a wideband ground-based microwave remote sensing system for vegetation monitoring in Malaysia. Previously, we had designed a C-Band FMCW radar system that operated in 582 MHz and the outcome of the system was encouraging. Therefore, a new wideband, VNA ground-based radar system is proposed to enhance the existing system.

VNA consists of four ports, operating from 300 Kz to 8 GHz, two wideband horn antennas, operating from 0.7 GHz to 7 GHz and an amplifier of 2 GHz to 26.5 GHz. The frequency range of 2 GHz–7 GHz is selected based on the lower limit of the microwave amplifier and the upper limit of the antennas. Apart from that, the in-house RF circuitry is designed based on the four linear polarimetric configuration (HH, VV, VH and HV). Figure 1 shows the block diagram of the proposed system. RF switch is used to perform the required several designated systems such as reference signal, Thru calibration signal and most importantly, the fully polarimetric measurement signal of the target area.

In this design, Port 1 is configured as output port, Port 2 is used as external reference channel, Port 3 and Port 4 are designated to measure the fully polarimetric signal of HH, VH, HV and VV from the target area through integrated RF circuit. As the system is installed on the mobile platform, 15 meters long cable is used to connect the VNA to the RF circuitry. RF cables with the length of 2 meters are also used to provide the linkage between RF circuitry to the antennas. The proposed wideband radar system is configured as a quasi monostatic radar system. The two antennas are placed 20 millimeters apart from each other. Such configuration allows better co-polarization and cross-polarization isolation as compared to the single antenna system.

The operation algorithm is scripted in a workstation to provide command and data storage to the system. With the Local Area Network/GPIB bus connection, the system is able to have better accessibility from various LAN connections. Besides, it is also

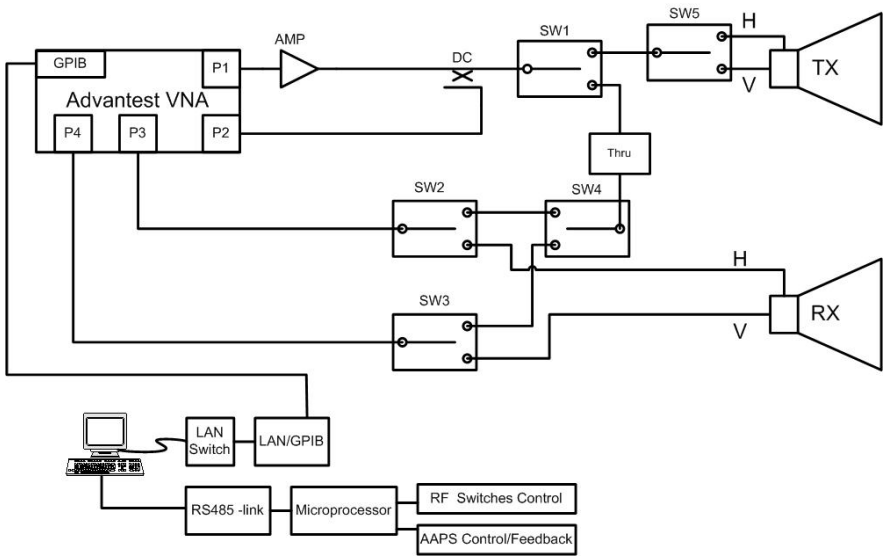

Figure 1. The block diagram of the proposed system.

configured with the AAPS to ease the measurement process. The AAPS is capable of providing two degrees of freedom to the position the antenna for data collection purpose.

With the data collected from the antenna, image reconstruction is performed to produce 3-D radar image. The reconstruction technique of Range Migration Algorithm involves four major steps. They include FFT, matched filtering, Stolt interpolation and IFFT. Apart from that, time gating, windowing and zero padding process are also important for pre-processing. Time gating procedure is very crucial so that the antenna coupled loss and unwanted range data can be filtered. It utilizes windowing function on time domain signal to reserve only the desire signals. The procedure can be formulate as

$$f(t) = f_o(t) * w(t) \tag{1}$$

where

$$\begin{aligned} f(t) &= \text{gated signal} \\ f_o(t) &= \text{original signal before gated} \\ w(t) &= \text{windowing function} \end{aligned}$$

Zero padding process helps to increase the length of the aperture and it has significant impact in improving the cross-range resolution.

Matched filtering, on the other hand, introduces compensation to wavenumber domain backscatter data. It corrects the wavefront curvature of all the scatterers at the same ground range as the scene centre. Prior to IFFT process, Stolt interpolation procedure is carried out to change the wavenumber domain to spatial frequency domain. Bypassing this interpolation procedure will cause blurring effect on the 3-D radar image.

3. REAL AND SYNTHETIC APERTURE RADAR MEASUREMENTS

To verify the system, a preliminary point target measurement has been done using the $8''$ sphere, $12''$ sphere and $\alpha = 0°$ and $\alpha = 45°$ oriented $4''\times8''$ dihedral corner reflector. It is performed in an open space during in situ measurement at rice field. The measured result is analyzed and compared with the theoretical value using time domain analysis of measured frequency domain radar cross section data [44].

Preliminary calibration process is done in two ways, namely static point target measurement and scanning measurement. For the static point target measurement, the AAPS is configured to stay at a specific location statically to point directly to the pedestal. Later, the AAPS is requested to scan along the linear actuator of the AAPS from the far right to the far left of the AAPS position. The measurement along the linear actuator is performing with the "stop and go algorithm"

Figure 2. Static point target measurement setup.

which will request the AAPS to stop at predefined steps and perform radar measurements. The static point target measurement setup is shown in Figure 2. The target pedestal is built using polystyrene and it is placed 5 meters away from antenna and 2 meters above the ground. The measured frequency point from the VNA is converted to backscattering coefficient versus range profile through Inverse Fast Fourier Transform and radar equation recalculation with a predefined gating.

In general, this calibration technique requires a theoretical known target to act as a reference target to obtain an error coefficient of the system. The generated error coefficient is used to convert the relative measurement data to absolute value. In this paper, $12''$ sphere is selected as the known target and $8''$ sphere is used as an unknown target. Firstly, the known target is measured and this is followed by the measurement of $8''$ sphere and pedestal. The pedestal measurement is then utilized for background subtraction during the calibration process. The calibration formula is as stated below:

$$\text{Absolute RCS value} = \frac{Unknown\ Target - Background}{Known\ Target - Background} \times Theoretical\ Value\ of\ Known\ Target \quad (2)$$

In order to remove the unwanted noise, time gating is essential to calculate the absolute unknown target value. The final output of the process is shown in Figure 3.

From Figure 3, the frequency response of $8''$ spheres follows the oscillating trend of the theoretical value. A close agreement between the measured and theoretical values is observed from 2 GHz to 4.2 GHz but there is a slight difference at the frequency region above 4.2 GHz. This is most likely due to the difference positioning level between two spheres and vibration caused by strong wind.

On the other hand, the scanning measurement involves integration of the proposed system and the AAPS to perform a series of measurement. The data collection geometry is given in Figure 4 and it shows the trajectory of the antenna during the scanning measurement process. Initially, the antenna moving tray is static at datum location of the AAPS. The AAPS is then moved to the far left during the initialization and the measurement begins from the far left to far right. The scanning measurement setup is shown in Figure 5. The measurement is carried out on a 45 days old rice field.

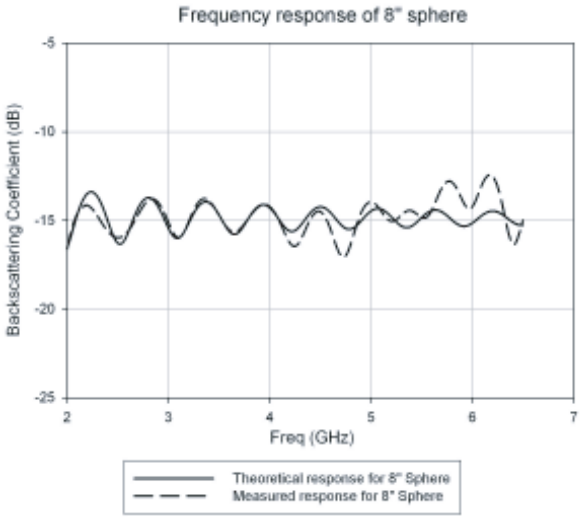

Figure 3. Frequency response of $8''$ sphere.

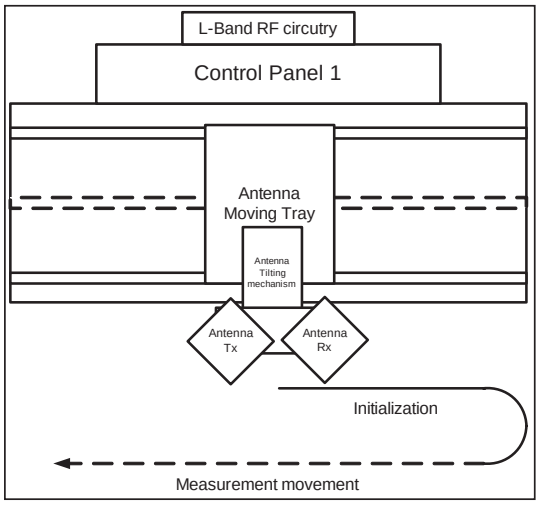

Figure 4. AAPS data collection geometry.

4. RESULTS AND DISCUSSION

The results of co-polarized for $8''$ sphere, $12''$ sphere, $\alpha = 0°$ oriented $4'' \times 8''$ Dihedral and the results of cross-polarized for $\alpha = 45°$ oriented $4'' \times 8''$ Dihedral are shown in Figure 6, Figure 7, Figure 8 and Figure 9

Figure 5. Scanning measurement setup.

respectively. They are selected based on characteristic of the radar point target with respect to co-polarized and cross-polarized signal. From these figures, slot time domain represents the AAPS scanning iteration of 41 samples across the linear scan and the range refers to the target range from the antenna.

The target responses of the $8''$ and $12''$ spheres show stable return across the scanning region. This is achieved by the wide beamwidth antenna that capable to obtain return signal from the spheres reflection. There is also slightly stronger target return at iteration of 20 in slow time domain for both $8''$ and $12''$ spheres. The $4'' \times 8''$ dihedral is used in this experiment due to its unique characteristic in transmitting strong target return at the orientation of $\alpha = 0^\circ$ or 90° for co-polarization and $\alpha = 45^\circ$ for cross-polarization.

The co-polarized results of the $4'' \times 8''$ dihedral at $\alpha = 0^\circ$ and the cross-polarized results at $\alpha = 45^\circ$ are shown in Figure 7 and Figure 8, respectively. This proves the functionality of the proposed system in measuring both co-polarized and cross-polarized signals. From the Figure 7, the proposed system is able to detect a strong target return from $\alpha = 0^\circ$ oriented $4'' \times 8''$ dihedral at the target range of 5 meters. A stronger target return is also shown in iteration No. 20 in slow time domain and the signal strength decreases when the antenna is moving

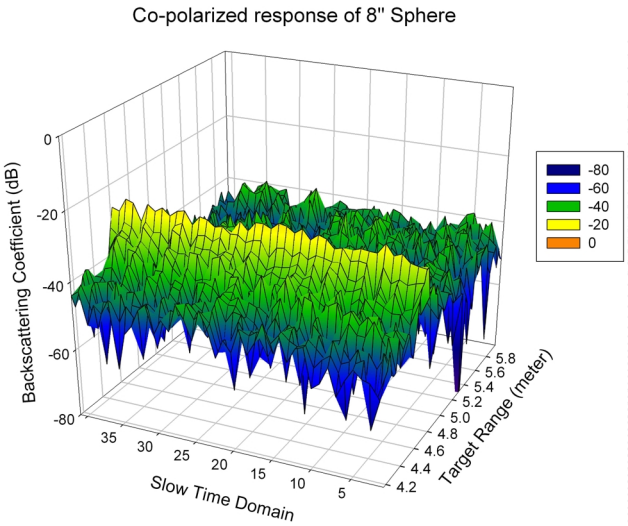

Figure 6. Co-polarized target return of $8''$ sphere in scanning measurement.

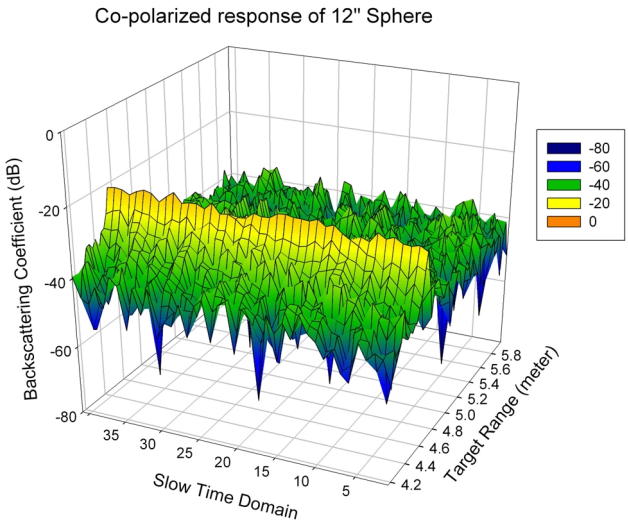

Figure 7. Co-polarized target return of $12''$ sphere in scanning measurement.

away from the center point. This is probably due to the characteristic of the $\alpha = 0^\circ$ oriented $4'' \times 8''$ dihedral where the target responses will decrease when the antenna front is moving away from the target.

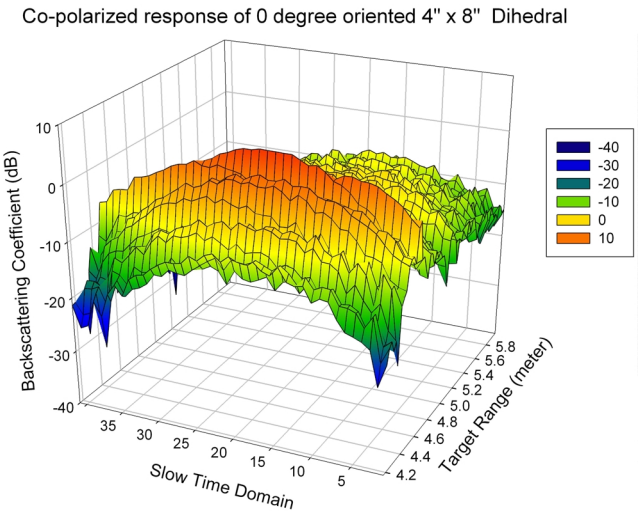

Figure 8. Co-polarized target return of 0° oriented $4'' \times 8''$ in scanning measurement.

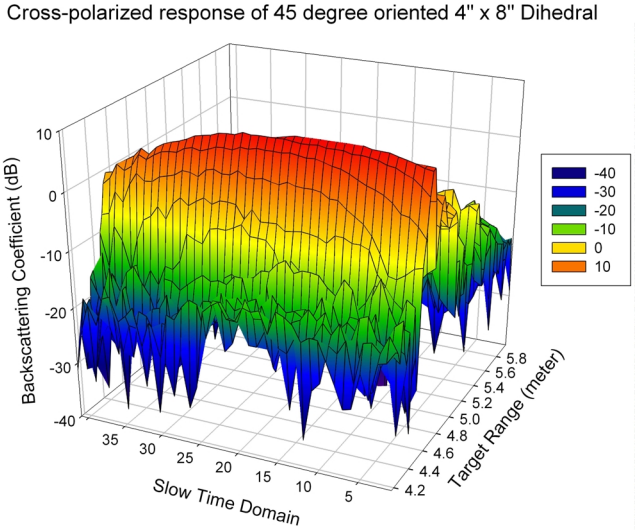

Figure 9. Cross-polarized target return of 45° degree oriented $4'' \times 8''$ in scanning measurement.

The cross polarized response of the $\alpha = 45^\circ$ oriented $4'' \times 8''$ in Figure 8 shows a strong return at target range of 5 meters. The results also portray stronger turn at iteration of 20 where the antenna

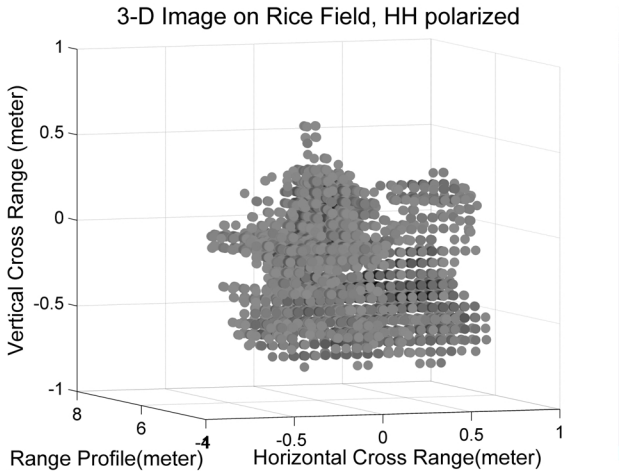

Figure 10. 3-D radar image of rice field for HH polarization.

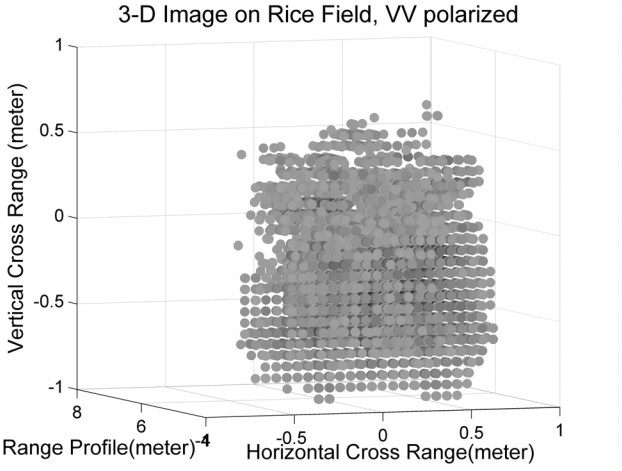

Figure 11. 3-D radar image of rice field for VV polarization.

is directly pointing to the target. The target response of cross polarized also follows the similar trend of $\alpha = 0^\circ$ oriented $4'' \times 8''$ dihedral where the target response decreases when the antenna is moving away from the target.

On the other hand, the implementation of 3-D imaging using RMA method is performed. The beauty of RMA is that it requires simple planar scan surface and it is suitable for near field application.

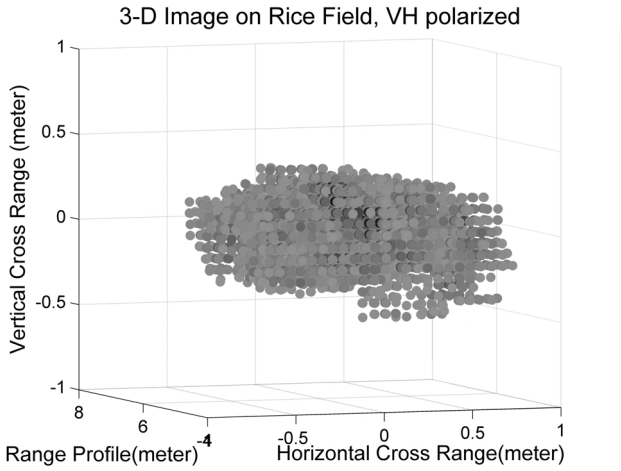

Figure 12. 3-D radar image of rice field for VH polarization.

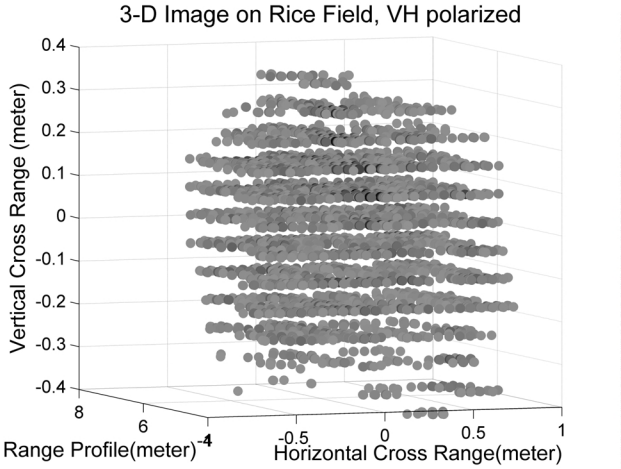

Figure 13. 3-D zoomed image of rice field for VH polarization.

The range resolution is determined by the bandwidth of the stepped frequency waveform while the cross-range resolution in horizontal axis and vertical axis are determined by the aperture length of planar scanner. The sample along the planar track is consistent throughout the measurement process. The result of the 3-D image of HH polarized, VV polarized and VH polarized are shown in Figure 10, Figure 11 and Figure 12, respectively.

In general, VV and HH polarized images show an orientation of evenly distributed scattering. This is probably due to the

backscattering return attenuated by the plant stems and the backscatter from the leaves. The intensity of VV polarized images is also found greater than the HH polarized and it is possibly due to the fact that the plant stems and leaves are majority vertical orientated at this early growth stages. For VH polarization, the 3-D radar image of the rice field shows less intensity compared to co-polarization images. On the other hand, from the zoomed image of VH polarization at the vertical cross range from -0.4 to 0.4 shown in Figure 13, it is found that the system is able to display a well organized 3-D scattering caused by the evenly grown plant.

5. CONCLUSION

A wideband VNA ground-based radar system has been proposed and constructed for the *in-situ* measurement for earth monitoring. Using time domain analysis for frequency based measured data, calibration has been done successfully. Calibrated target return in frequency domain showed an acceptable range response and the continuation of calibration work will be performed in near future to obtain better results. The target range profile has been measured using the integrated wideband radar system and the operation of AAPS proved the advantages of automation in RCS measurement, especially in outdoor environment. Graphical representation of real aperture radar was obtained with this configuration and the preliminary results of the 3-D image reconstruction of the rice field was shown using Range Migration Algorithm. The results of the integrated system showed a strong confidence level that the system is ready for various environmental monitoring activities such as vegetation growth monitoring, surface roughness study and man made target analysis. The proposed system is also served as a platform to develop a better ground-based remote sensing technology.

ACKNOWLEDGMENT

This work has been funded by the Malaysian Remote Sensing Agency (MACRES). The authors would like to thank the officers from MACRES and Ministry of Agriculture for the immeasurable support.

REFERENCES

1. Rakotoarivony, L., O. Taconet, D. Vidal-Madjar, P. Bellemain, and M. Benallegue, "Radar backscattering over agricultural

bare soils," *Journal of Electromagnetic Waves and Applications*, Vol. 10, No. 2, 187–209, 1996.

2. Alejandro, M., I. Chenerie, F. Baup, E. Mougin, and K. Sarabandi, "Angular normalization of ENVISAT ASAR data over Sahelian grassland using a coherent scattering model," *PIERS Online*, Vol. 2, No. 1, 94–98, 2006.
3. Koay, J. Y., C. P. Tan, K. S. Lim, S. Bahari, H. T. Ewe, H. T. Chuah, and J. A. Kong, "Paddy fields as electrically dense media: Theoretical modeling and measurement comparisons," *IEEE Transactions on Geoscience and Remote Sensing*, Vol. 45, No. 9, 2837–2849, 2007.
4. Koay, J.-Y., C. P. Tan, S. Bahari, H.-T. Ewe, and H.-T. Chuah, "Theoretical modeling and measurement comparison of season-long rice field monitoring," *PIERS Online*, Vol. 1, No. 1, 25–28, 2005.
5. Lim, K.-S., C.-P. Tan, J.-Y. Koay, V. C. Koo, H.-T. Ewe, Y.-C. Lo, and A. Ali, "Multitemporal C-band radar measurement on rice fields," *PIERS Online*, Vol. 3, No. 1, 44–47, 2007.
6. Tan, C.-P., J.-Y. Koay, K.-S. Lim, H.-T. Ewe, and H.-T. Chuah, "Classification of multi-temporal SAR images for rice crops using combined entropy decomposition and support vector machine technique," *Progress In Electromagnetics Research*, PIER 71, 19–39, 2007.
7. Paris, J. F., "Active microwave properties of vegetation," *Fund. Remote Sensing Sci. Res. Program, 1985 Summary Report of the Scene Radiation and Atmos. Effects Characterization Project*, D. Deering (ed.), 148–154, NASA TM 86234, MIT, Cambridge, MA, 1985.
8. Boyarskii, D. A., V. V. Tikhonov, and N. Yu. Komarova, "Model of dielectric constant of bound water in soil for applications of microwave remote sensing," *Progress In Electromagnetics Research*, PIER 35, 251–269, 2002.
9. Nghiem, S. V., M. Borgeaud, J. A. Kong, and R. T. Shin, "Polarimetric remote sensing of geophysical media with layer random medium model," *Progress In Electromagnetics Research*, PIER 03, 1–73, 1990.
10. Shin, R. T. and J. A. Kong, "Radiative transfer theory for active remote sensing of two-layer random medium," *Progress In Electromagnetics Research*, PIER 01, 359–417, 1989.
11. De Badereau, D., H. Roussel, and W. Tabbara, "Radar remote sensing of forest at low frequencies: A two dimensional full wave approach," *Journal of Electromagnetic Waves and Applications*,

Vol. 17, No. 6, 921–949, 2003.

12. Angot, L., H. Roussel, and W. Tabbara, "A full wave three dimensional analysis of forest remote sensing using VHF electromagnetic wave," *Progress In Electromagnetics Research*, PIER 38, 311–331, 2002.
13. Lopez-Sanchez, J. M., J. Fortuny-Guasch, S. R. Cloude, and A. J. Sieber, "Indoor polarimetric radar measurements on vegetation samples at L, S, C and X band," *Journal of Electromagnetic Waves and Applications*, Vol. 14, No. 2, 205–231, 2000.
14. Koo, V. C., Y. K. Chan, G. Vetharatnam, T. S. Lim, B.-K. Chung, and H.-T. Chuah, "The MASAR project: Design and development," *Progress In Electromagnetic Research*, PIER 50, 279–298, 2005.
15. Picard, G. and T. Le Toan, "A multiple scattering model for C band backscatter of wheat canopies," *Journal of Electromagnetic Waves and Applications*, Vol. 16, No. 10, 1447–1466, 2002.
16. De Matthaeis, P. and R. H. Lang, "Microwave scattering models for cylindrical vegetation components," *Progress In Electromagnetics Research*, PIER 55, 307–333, 2005.
17. Le Toan T., A. Lopes, and M. Huet, "On the relationships between radar backscattering coefficient and vegetation canopy characteristics," *Proc. IGARSS*, 155–160, Strasbourg, France, Aug. 1984.
18. Ulaby, F., R. Moore, and A. K. Fung, *Microwave Remote Sensing: Active and Passive*, Vol. 3, Artech House, Norwood, MA, 1986.
19. Bouman, B. A. and D. K. Hoekman, "Multitemporal, multi-frequency radar measurements of agricultural crops during the Agriscat-88 campaign in The Netherlands," *International Journal of Remote Sensing*, Vol. 14, No. 8, 1595–1614, 1993.
20. Zoughi, R., L. K. Wu, and R. K. Moore, "Identification of major backscattering sources in trees and shrubs at 10 GHz," *Remote Sensing Environment*, Vol. 19, No. 3, 269–290, 1986.
21. Wu, L. K., R. K. Moore, R. Zoughi, A. Afifi, and F. T. Ulaby, "Preliminary results on the determination of the sources of scattering from vegetation canopies at 10 GHz," *International Journal of Remote Sensing*, Vol. 6, No. 2, 299–313, 1985.
22. Paris, J. F., "Characterization of cultural deciduous trees, grapes, and irrigated crops with radar and optical remote sensing," *Ann. Rep., Microwave-Optical Characterization of Vegetation with Remote Sensing Project*, NASA Lyndon B. Johnson Space Center,

Houston, TX, 1985.

23. Paris, J. F., "Radar scatterometer probing of thick vegetation canopies," *International Geoscience Remote Sensing Symposium*, Vol. 1, 161–163, 1985.
24. Pitts, D. E., G. D. Badhwar, and E. Reyna, "Estimation of biophysical properties of forest canopies through inversion of microwave scatterometer data," *International Geoscience Remote Sensing Symposium*, Vol. 1, 313–320, 1985.
25. Wu, S. T., "A preliminary report on the measurements of forest canopies with C-band radar scatterometer at NASA/NSTL," *International Geoscience Remote Sensing Symposium*, Vol. 2, 168–173, 1985.
26. Le Toan T., H. Laur, E. Mougin, and A. Lopes, "Multitemporal and dual-polarization observations of agricultural vegetation covers by X-band SAR images," *IEEE Transactions on Geoscience and Remote Sensing*, Vol. 27, 709–717, 1989.
27. Le Toan T., F. Ribbes, L. F. Wang, N. Floury, K. H. Ding, J. A. Kong, M. Fujita, and T. Kurosu, "Rice crop mapping and monitoring using ERS-1 data based on experiment and modeling results," *IEEE Transactions on Geoscience and Remote Sensing*, Vol. 35, 41–56, 1997.
28. Kurosu, T., M. Fujita, and K. Chiba, "Monitoring of rice crop growth from space using ERS1 C-band SAR," *IEEE Transactions on Geoscience and Remote Sensing*, Vol. 33, 1092–1096, 1995.
29. Kim, S. B., B. W. Kim, Y. K. Kong, and Y. S. Kim, "Radar backscattering measurements of rice crop using X-band scatterometer," *IEEE Transactions on Geoscience and Remote Sensing*, Vol. 38, 1467–1471, 2000.
30. Koo, V. C., B. K. Chung, and H. T. Chuah, "Development of a ground-based radar for scattering measurements," *IEEE Antennas and Propagation Magazine*, Vol. 45, No. 2, 36–42, 2003.
31. Koo, V. C., B. K. Chung, and H. T. Chuah, "Design and development of a scatterometer system for environmental monitoring," *Proceeding of IGARSS 1999 Symposium*, Hamburgh, Germany, 1999.
32. Soumekh, M., *Synthetic Aperture Radar Signal Processing with Matlab Algorithms*, John Wiley & Son, 1999.
33. Jin, M. Y., F. Cheng, and M. Chen, "Chirp scaling algorithm for SAR processing," *IEEE International Geoscience and Remote Sensing Symposium, IGARSS '93*, Vol. 3, 1169–1172, 1993.
34. Lopez-Sanchez, M. and J. Fortuny-Guasch, "3-D radar imaging

using range migration techniques," *IEEE Transactions on Antennas and Propagations*, Vol. 48, No. 5, May 2000.

35. Cafforio, C., C. Prati, and E. Rocca, "SAR data focusing using seismic migration techniques," *IEEE Transactions on Aerospace and Electronic Systems*, Vol. 27, No. 2, 1991.
36. Fortuny-Guasch, J. and M. Lopez-Sanchez, "Extension of 3-D range migration algorithm to cylindrical and spherical scanning geometries," *IEEE Transactions on Antennas and Propagations*, Vol. 49, No. 10, 2001.
37. Chiang, C. T. and B. K. Chung, "High resolution 3-D imaging," *3rd National Microwave Remote Sensing Seminar*, 2004.
38. Chan, Y. K. and V. C. Koo, "An introduction to synthetic aperture radar," *Progress In Electromagnetics Research B*, Vol. 2, 27–60, 2008.
39. Chan, Y. K. and S. Y. Lim, "Synthetic aperture radar (SAR) signal generation," *Progress In Electromagnetics Research B*, Vol. 1, 269–290, 2008.
40. Storvold, R., E. Malnes, Y. Larsen, K. A. Hogda, S.-E. Hamran, K. Mueller, and K. Langley, "SAR remote sensing of snow parameters in norwegian areas — Current status and future perspective," *Journal of Electromagnetic Waves and Applications*, Vol. 20, No. 13, 1751–1759, 2006.
41. Oka, S., H. Togo, N. Kukutsu, and T. Nagatsuma, "Latest trends in millimeter-wave imaging technology," *Progress In Electromagnetics Research Letters*, Vol. 1, 197–204, 2008.
42. Ma, C. Z., T. S. Yeo, H. S. Tan, and G. Lu, "Interferometric ISAR imaging on squint model," *Progress In Electromagnetics Research Letters*, Vol. 2, 125–133, 2008.
43. Lim, T. S., V. C. Koo, H.-T. Ewe, and H.-T. Chuah, "A SAR autofocus algorithm based on particle swarm optimization," *Progress In Electromagnetics Research B*, Vol. 1, 159–176, 2008.
44. Lim, T. S., C.-S. Lim, V. C. Koo, H.-T. Ewe, and H.-T. Chuah, "Autofocus algorithms performance evaluations using an integrated SAR product simulator and processor," *Progress In Electromagnetics Research B*, Vol. 3, 315–329, 2008.
45. Jersak, B. D., M. Dolaty, and A. J. Blanchard, "Time domain enhancement of frequency domain radar cross-section data," *International Journal of Remote Sensing*, Vol. 13, No. 11, 2105–2119, 1992.